AMERICAN SOCIETY FOR MICROBIOLOGY | Journal of Virology®

VIRUS-CELL INTERACTIONS

Interferon Gamma Prevents Infectious Entry of Human Papillomavirus 16 via an L2-Dependent Mechanism

Patricia M. Day, Cynthia D. Thompson, Douglas R. Lowy, John T. Schiller

Laboratory of Cellular Oncology, NCI, NIH, Bethesda, Maryland, USA

ABSTRACT In this study, we report that gamma interferon (IFN-γ) treatment, but not IFN-α, -β, or -λ treatment, dramatically decreased infection of human papillomavirus 16 (HPV16) pseudovirus (PsV). In a survey of 20 additional HPV and animal papillomavirus types, we found that many, but not all, PsV types were also inhibited by IFN-γ. Microscopic and biochemical analyses of HPV16 PsV determined that the antiviral effect was exerted at the level of endosomal processing of the incoming capsid and depended on the JAK2/STAT1 pathway. In contrast to infection in the absence of IFN-γ, where L1 proteolytic products are produced during endosomal capsid processing and L2/DNA complexes segregate from L1 in the late endosome and travel to the nucleus, IFN-γ treatment led to decreased L1 proteolysis and retention of L2 and the viral genome in the late endosome/lysosome. PsV sensitivity or resistance to IFN-γ treatment was mapped to the L2 protein, as determined with infectious hybrid PsV, in which the L1 protein was derived from an IFN-γ-sensitive HPV type and the L2 protein from an IFN-γ-insensitive type or vice versa.

IMPORTANCE A subset of HPV are the causative agents of many human cancers, most notably cervical cancer. This work describes the inhibition of infection of multiple HPV types, including oncogenic types, by treatment with IFN-γ, an antiviral cytokine that is released from stimulated immune cells. Exposure of cells to IFN-γ has been shown to trigger the expression of proteins with broad antiviral effector functions, most of which act to prevent viral transcription or translation. Interestingly, in this study, we show that infection is blocked at the early step of virus entry into the host cell by retention of the minor capsid protein, L2, and the viral genome instead of trafficking into the nucleus. Thus, a novel antiviral mechanism for IFN-γ has been revealed.

KEYWORDS HPV, papillomavirus, interferon, IFN-γ, L2

Received 30 January 2017 **Accepted** 26 February 2017

Accepted manuscript posted online 1 March 2017

Citation Day PM, Thompson CD, Lowy DR, Schiller JT. 2017. Interferon gamma prevents infectious entry of human papillomavirus 16 via an L2-dependent mechanism. J Virol 91: e00168-17. https://doi.org/10.1128/JVI.00168-17.

Editor Lawrence Banks, International Centre for Genetic Engineering and Biotechnology

Address correspondence to Patricia M. Day, pmd@nih.gov.

Papillomaviruses (PV) are members of a large group of nonenveloped DNA tumor viruses that infect epithelial tissues of a wide range of vertebrate species. A subset of oncogenic mucosal human PV (HPV) types are the causal agents of cervical cancer. These high-risk types, especially HPV16, are also linked to vulvar, vaginal, anal, and oropharyngeal cancers (1). The cascade of viral protein expression is integrally tied to epithelial differentiation, with virion production only occurring in the terminally differentiated upper layers (2). These features combine to allow circumvention of host innate and adaptive immune responses, as few proinflammatory signals are elicited during these early stages (3). However, most PV infections that induce overt hyperproliferation are eventually cleared with the apparent involvement of lymphocytic infiltrates (reviewed in reference 4). Also, HPV infections are often superimposed on colonization with other microbial agents, e.g., in the female reproductive tract (reviewed in reference 5). It is, therefore, of interest to determine if antiviral molecules that are known components of the innate or adaptive immune response to other infections could

inhibit PV infection. In this regard, there has been a single report of type I interferons inhibiting *in vitro* HPV16 infection (6).

The IFNs are a family of secreted polypeptides that were first identified by their ability to induce cellular resistance to viral infection (7). Type I interferons, including IFN-α and IFN-β, are released from many virus-infected cells and interact with a shared, broadly expressed plasma membrane receptor (8, 9). The more recently described type III IFNs (IFN-λ) are also induced by viral infection (10). However, IFN-λ receptors are largely restricted to cells of epithelial origin, resulting in a narrower cellular response to pathogens (9). The sole type II IFN, IFN-γ, is released from activated T lymphocytes and NK cells (9). IFN-γ is critical for macrophage activation in response to microbial infection, but a wide variety of other cell types, including epithelial cells, express its receptor, IFNGR, and are responsive to IFN-γ activation (8, 9). The antiviral activity of IFN-γ can either occur directly through the induction of effector molecules or indirectly through enhanced antigen presentation.

One technical consequence of the restriction of the productive PV life cycle to the terminally differentiating epithelium is the resultant difficulty in obtaining authentic viral particles. The pseudovirus (PsV) production system, which is an alternative to authentic virus, has been used most often to examine early events in PV infection, including host cell binding and entry (11–13). These surrogate particles contain the two capsid proteins, the major protein, L1, and the minor protein, L2, and encapsidate a plasmid termed a pseudogenome, which encodes a reporter protein. Expression of this reporter indicates successful completion of the entry process. PV initially interact with heparan sulfate proteoglycans (HSPGs) on either the cell surface (*in vitro*) or basement membrane (*in vivo*) (14–16). This interaction induces distinct conformational changes in the capsids, including the critical exposure of the amino terminus of L2, which contains a conserved furin cleavage site that must be proteolytically processed for successful infection (17, 18). Capsid endocytosis proceeds via a novel pathway which is most closely related to macropinocytosis (19). The viral particles traverse the endosomal system via early endosomes and are subsequently delivered to late endosomes (LE)/lysosomes (20, 21). In the presence of lysosomotropic agents, infection is abolished, and the particles accumulate in the LE/lysosomal compartment (19). The majority of the major capsid protein, L1, is retained within this compartment, whereas L2 and the genome are segregated from L1 and delivered into the *trans*-Golgi network (TGN) via a Rab7b- and Rab9a-dependent manner prior to their delivery to the nucleus (22). Retromer-dependent transport of the L2/DNA complex from the early endosome has also been presented as an alternative mode of entry to the TGN (23, 24). Entry into the nucleus requires mitosis, after which the L2/DNA complex localizes to the subnuclear domain ND10, where transcription of the virally delivered DNA can occur (25, 26).

In this study, we have evaluated the effect of various classes of IFNs on HPV PsV infection *in vitro*. Although many studies have examined the consequences of various IFNs on overall replication of a range of viruses, very few reports have examined the effects of IFNs on the early stages of the viral life cycle in which the PsV participate. Our study documents potent inhibition of many, but not all, HPV PsV by IFN-γ but not other IFNs.

RESULTS

IFN-γ efficiently prevents HPV16 PsV infection. We utilized HPV16 pseudovirus (PsV) infection to assess possible antiviral effects of various exogenous IFNs on the early stages of HPV infection. These experiments were performed in HaCaT cells, a spontaneously transformed human keratinocyte cell line that is often utilized for PV entry analyses. Treatment of cells with 10 ng/ml IFN-γ resulted in a dramatic decrease in HPV16 PsV infection, as measured by expression of the GFP-encoding expression plasmid packaged by the PsV (Fig. 1A). Unexpectedly, treatment with 5 other IFN types at the same concentration did not affect PsV infection. These negative results included several repeat experiments in which treatment with IFN-α and IFN-β, the IFN types reported previously to inhibit HPV16 PsV infection (6), were tested. For these

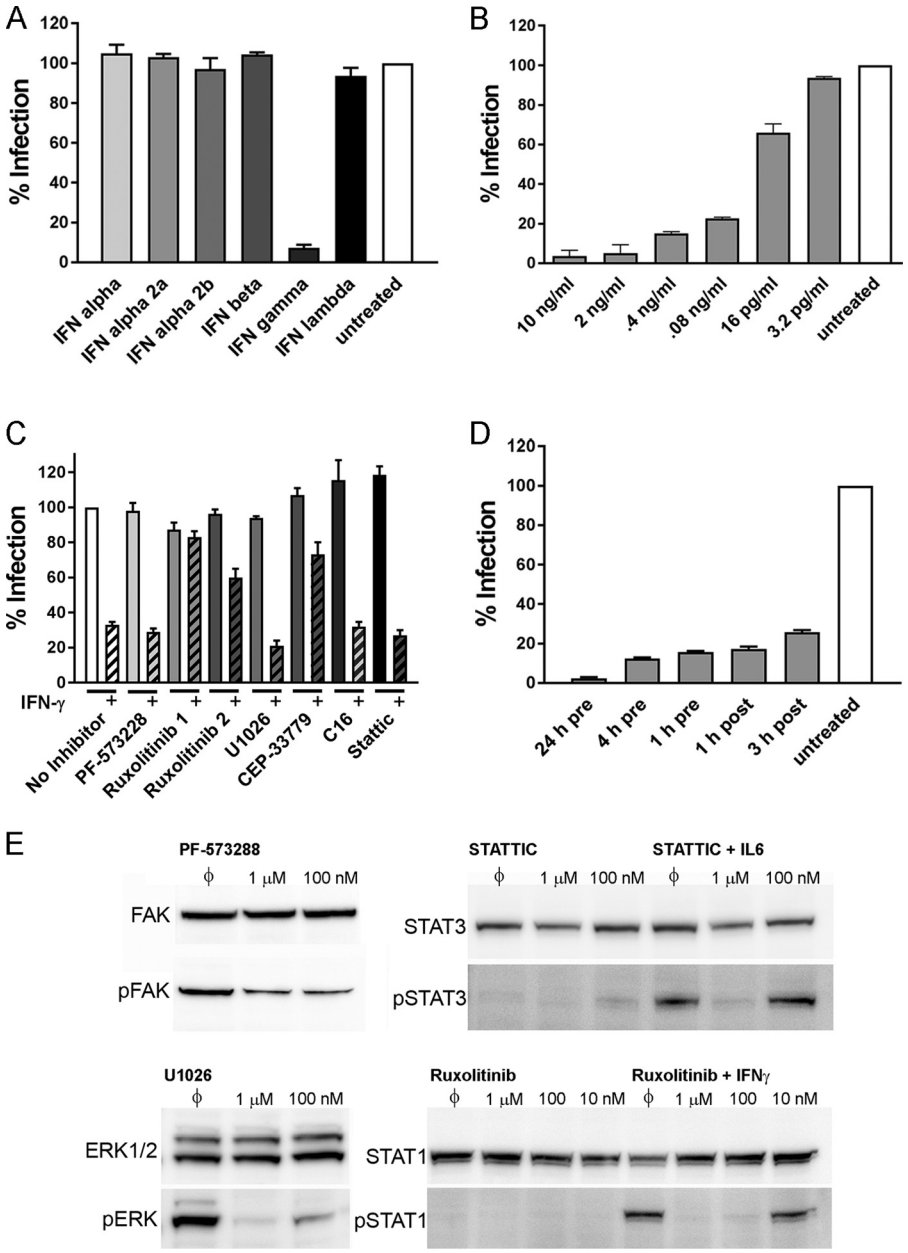

FIG 1 HPV16 PsV infection of HaCaT cells is sensitive to type II IFN treatment. (A) HaCaT cells were treated with 10 ng/ml of various types of IFN for 18 h prior to infection with an HPV16 PsV that contained a packaged GFP expression plasmid. GFP expression was determined by flow-cytometric analysis at 72 h postinfection. The percentage of infection in untreated cells was set to 100%. The percentage of infection in the treated samples was normalized to that value. Triplicate infections were analyzed for all experiments. (B) The amount of IFN-γ necessary to decrease HPV16 PsV infection was determined by titration. The noted amount of IFN-γ was added to cells 18 h prior to commencement of infection. Inhibition data were normalized to untreated, infected cells. (C) Inhibitors were added immediately prior to IFN-γ addition (0.2 ng/ml) or analyzed in the absence of activation. The unlined bars indicate infection with the inhibitor only, and the lined bars in the same color shade indicate the data with IFN-γ activation. The data are normalized to the infection levels in untreated, HPV16 PsV-infected cells. The inhibitors were used at the following concentrations: PF-573228, 100 nM; ruxolitinib 1, 1 μM; ruxolitinib 2, 100 nM; U1026, 100 nM; CEP-33779, 20 nM; C16, 1 μM, stattic, 1 μM. As noted in the text, only treatment with ruxolitinib and CEP-33779 repressed the IFN-γ effect on HPV16 PsV infection. (D) IFN-γ (5 ng/ml) was added at different times pre- or postinfection with HPV16 PsV, as indicated, and infection data were normalized to untreated, infected cells. (E) The efficacy of the inhibitors at the concentrations utilized for panel C were evaluated by examination of the phosphorylation status of the target protein as indicated. To induce STAT3 phosphorylation, cells were treated with 20 ng of IL-6 for 15 min following addition of stattic. Both concentrations of ruxolitinib shown in panel C were evaluated for their ability to block STAT1 phosphorylation. A lower concentration (10 nM) was found to be inefficient.

experiments, we used the same IFN source, cell line, and treatment time as in the earlier publication.

We next evaluated the dose dependence of IFN-γ on the inhibition of HPV16 PsV infection by performing a titration of the concentration of IFN-γ from 10 ng/ml to 3.2 pg/ml (Fig. 1B). Infection was inhibited even at low levels of exogenous IFN-γ, with substantial effects evident with a dose as low as 0.08 ng/ml. Comparable levels can be present in the local environment during the course of a microbial infection, as occurs following herpes simplex type 2 infection of the vaginal tract (27–29).

IFN-γ exerts its effect on cells by engagement of its receptor, IFNGR, which typically activates the Janus kinase (JAK) signal transducer and activator of transcription (STAT) intracellular signal transduction pathway, resulting in the transcriptional activation of IFN-γ-inducible genes (reviewed in reference 30). Inhibitors of this canonical signaling pathway include a pan-JAK inhibitor, ruxolitinib, and a JAK2-specific inhibitor, CEP-33779. In addition, IFN-γ may activate JAK-independent pathways. For example, in response to IFN-γ, there may be activation of the signal transduction cascade that includes the mitogen-activated protein kinase kinase 1 (MEKK1), the mitogen-activated protein kinase 1 (MEK1), and the extracellular signal-regulated kinases 1 and 2 (ERK1/2), which regulate the CCAAT/enhancer binding protein beta (C/EBP-beta) and C/EBP-beta-driven expression (31, 32). It has also been shown that IFN-γ can trigger the phosphorylation of MEKK4 through activation of Pyk2 (FAK2) in HaCaT cells (33). To determine which IFN-γ-induced pathway was responsible for the observed reduction of HPV16 PsV infection, we treated HaCaT cells with inhibitors of these pathways prior to IFN-γ addition and evaluated the subsequent effect on HPV16 PsV infection (Fig. 1C). For this experiment, we used a lower concentration of IFN-γ (0.2 ng/ml), which, because it inhibited infection less completely than the higher concentration, made it possible to identify either an increase in infection, indicating that the inhibitor blocked the IFN-γ pathway of interest, or a further reduction of infection, indicating the inhibitor cooperated with the effects of IFN-γ. None of the inhibitors had a dramatic effect on HPV16 PsV infection in the absence of IFN-γ treatment, implying that under our normal growth conditions, PsV infection does not utilize the pathways affected by the inhibitors (solid bars). In the presence of IFN-γ (lined bars), none of the inhibitors augmented the anti-PsV activity of IFN-γ. However, the two JAK inhibitors (ruxolitinib, at the two concentrations shown, and CEP-33779) largely reversed the negative effect of IFN-γ on PsV infection. These results indicate that the ability of IFN-γ to inhibit PsV infection depends on the canonical JAK2/STAT1 pathway. In contrast, there was no effect on the IFN-γ-induced phenotype when MEK1/2 was inhibited with U1026, FAK was inhibited with PF-573228, or STAT3 was inhibited by stattic, indicating that these pathways are not critical mediators of the reduction in PsV infection induced by IFN-γ. The efficacy of these inhibitors in HaCaT cells at the chosen concentrations was confirmed (Fig. 1E). The phosphorylation of FAK was incompletely blocked by PF-573228; however, we expect that this level of reduction would have been sufficient to be reflected in a functional decrease (Fig. 1C).

To determine the stage of PsV infection that was the target of the observed antiviral effect, we added IFN-γ to the HaCaT cells at different time points prior to or after HPV16 PsV addition (Fig. 1D). We found that we could still prevent almost 80% of PsV infection when we delayed addition of IFN-γ until 3 h postpseudovirus addition. HPV exhibits a slow asynchronous entry with a half time of 4 to 11 h. Thus, the inhibition kinetics led us to examine whether IFN-γ treatment affected the endocytic entry of the pseudovirus.

IFN-γ affects endocytic trafficking of HPV16 PsV. To evaluate the possibility that IFN-γ treatment affects HPV16 entry in HaCaT cells, we compared the localization of internalized HPV16 PsV at 24 h postinfection in untreated cells with that of cells that were treated with IFN-γ starting 18 h prior to infection. Consistent with previous studies, HPV16 L1 was localized in LE/lysosomes in the absence of IFN-γ (Fig. 2A), and this pattern was even more pronounced in the IFN-γ-treated cells (Fig. 2B). IFN-γ

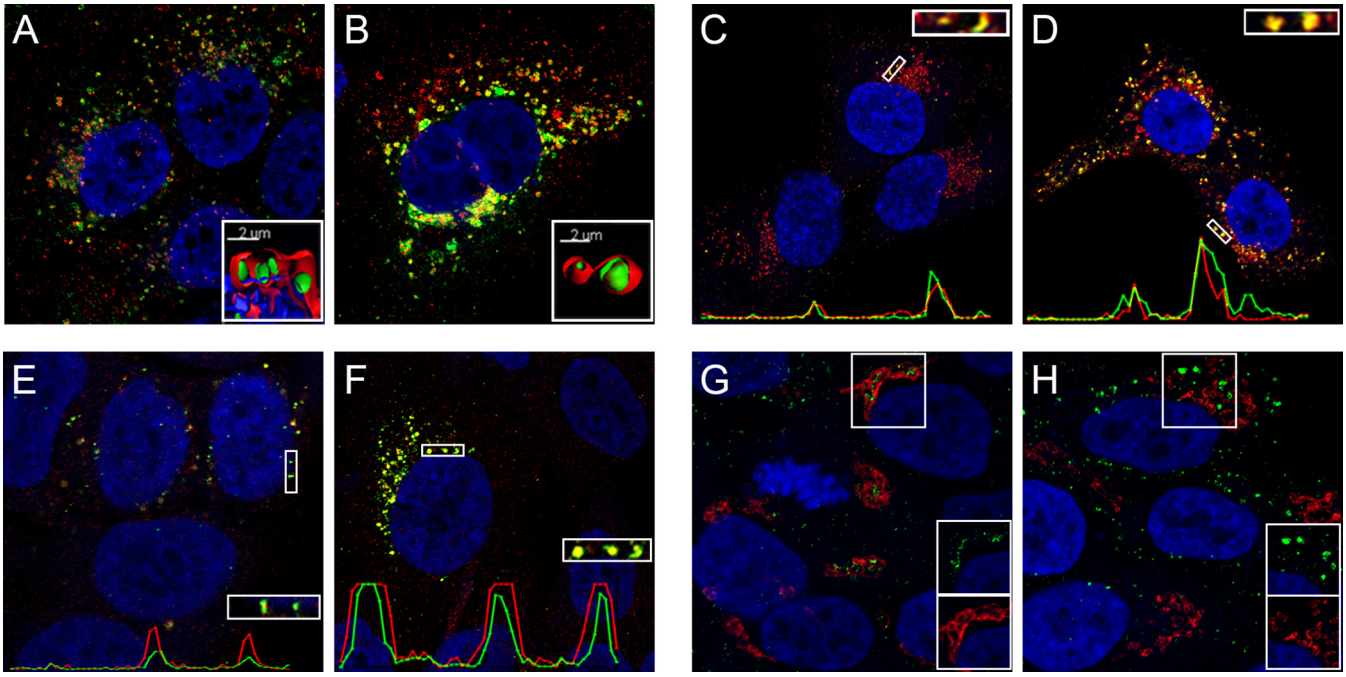

FIG 2 Viral components do not exit the LE in IFN-γ-treated cells. The localization of HPV16 PsV components was compared in untreated HaCaT cells and IFN-γ-treated cells at 24 h postinfection. IFN-γ-treated cells were treated for 18 h prior to virus addition. In all instances, the IFN-γ-treated condition is shown in the second panel of the pair. Panels A and B show the staining of HPV16 L1 in the green channel and the lysosomal protein LAMP-1 in the red channel. Note the increased staining intensity and colocalization in the IFN-γ-treated cells in panel B. The inset in each of these panels shows a surface-rendered image of a Z-stack series of each condition. Panels C and D show the localization of the delivered PsV genome in the green channel and L1 protein in the red channel. In order to appreciate the intensity of the vesicular staining under each condition, we have examined a line profile across a 7-μm region and inserted this within the panel along with a magnification of this region. The *y* axis reflects the pixel intensity across the distance (*x* axis). The third group, shown in panels E and F, show the colocalization of the PsV genome (green) and L2 protein (red). The line profiles for a chosen region have been inserted. In the final group (panels G and H), the Golgi localization of L2 was evaluated by costaining of L2 (green) with giantin (red). A split image of a chosen region is shown to allow better appreciation of the localization of L2 staining relative to the medial Golgi marker.

treatment seemed to cause an increase in the size of the LAMP-1-staining compartment in addition to the increased retention of PsV capsids within this compartment. To examine this, we measured the diameter of 50 LE/lysosomes for each condition. The range for untreated cells was 0.712 μm to 1.34 μm, with an average of 1.012 ± 0.0201 μm. For IFN-γ-treated cells the diameter range was 0.933 μm to 3.22 μm, with an average of 1.366 μm ± 0.0579 ($P < 0.0001$). This increased size can also be appreciated in the insets shown in Fig. 2A and B, which show the localization of HPV16 within the LAMP-1 compartment in both instances. We also examined the trafficking of the encapsidated pseudogenome, using HPV16 PsV particles that had packaged an 5-ethynyl-2′-deoxyuridine (EdU)-containing plasmid, which can localize the PV pseudogenome during entry. At the 24-h postinfection time point in untreated cells, most of the genome typically had left the endosomal system. The residual vesicular genome colocalizes with L1 (Fig. 2C). In contrast, the IFN-γ-treated cells demonstrated both increased retention of the genome with L1 as well as stronger staining overall, probably indicating a decreased loss of genome during capsid processing (Fig. 2D). The insets in Fig. 2C and D show a region at higher magnification, and the corresponding line profile at the bottom of the two panels verifies the colocalization of the vesicular genome with L1 in both instances and the increased signal intensity under the IFN-γ-treated conditions.

The subcellular distribution of L2 ordinarily mirrors that of the pseudoviral DNA, as both of these PsV components traffic together through the endosomes and TGN en route to ND10 (25). In untreated cells, these components were colocalized and distributed among the endosomes, the TGN, and ND10 at the 24-h time point, as previously described (Fig. 2E) (22). In contrast, although L2 and the pseudogenome were also colocalized in the IFN-γ-treated cells, there was no nuclear staining or Golgi-like pattern

(Fig. 2F), and all of the signal was apparently vesicular, as also demonstrated by the staining shown in Fig. 2B and D. The insets in Fig. 2E and F contain a magnified region, and the corresponding line profile confirms an increased signal intensity following IFN-γ treatment. We also examined the delivery of L2 to the Golgi complex. We have previously shown that L2 localizes to the TGN, adjacent to the medial Golgi marker protein giantin, during infectious entry (22). This localization was readily seen in the untreated cells (Fig. 2G). In contrast, in the IFN-γ-treated cells, the distribution of L2 was clearly distinct from the Golgi complex (Fig. 2H). The insets show the single-channel signals for the indicated region. To further demonstrate the deficiency in L2 delivery to the Golgi complex, we quantified the percentage of L2-positive cells that showed Golgi localization (100 $L2^+$ cells were examined for each condition). We found that only 13% of the IFN-γ-treated cells, compared to 64% of the control cells, had Golgi complex-localized L2. In sum, the microscopic analysis indicated that IFN-γ treatment caused the retention of L2 and packaged DNA in the LE/lysosomal compartment, where they continued to be colocalized with L1.

IFN-γ treatment affects vesicular processing of HPV16 capsids but does not globally affect endocytic trafficking. The proteolytic processing of HPV16 capsids during cell entry, as recently analyzed in detail by Cerqueira et al., results in distinct L1 cleavage products that are generated through protease cleavage during endosomal trafficking (34). To determine if IFN-γ activation altered this process, we added HPV16 PsV to untreated or IFN-γ-treated cells and examined L1 degradation during the initial 48 h of infection. We obtained similar results whether the L1 cleavage products were analyzed directly by Western blotting or immunoprecipitated with an anti-L1 polyclonal antiserum and then detected by Western blotting with an anti-L1 monoclonal antibody. We focused on the immunoprecipitation/Western blotting procedure (Fig. 3A), as this technique eliminates detection of the multiple reactive cellular proteins in HaCaT cells that, as described by Cerqueira et al., can interfere with analysis of the processed capsids by direct Western blotting (34). However, the heavy- and light-chain antibodies (labeled H and L, respectively) from the immunoprecipitation step are visible in all samples, including the cell-only control. In untreated cells, as previously reported, a ladder of less-than-full-length L1-derived products, migrating between approximately 23 kDa and 45 kDa, was seen at the 6-h time point, and these products were resolved at the 24- and 48-h time points with the coincident appearance of a lower product of approximately 15 kDa. In the IFN-γ-treated cells, however, the processing was less extensive. The ~23-kDa doublet in the IFN-γ-treated cells was less prominent at 6 h than in the untreated control at this time point, but the intensity of the doublet was increased at 24 and 48 h, making it similar to that of the untreated control at 6 h and more intense than the untreated control at the later time points. Furthermore, there was no decrease over time in the slower-migrating degradation products, and only a trace of the ~15-kDa product was seen. These results indicate that the endocytic processing of HPV16 pseudovirions is impaired following IFN-γ treatment. It should also be noted that this pattern does not resemble those observed previously with a panel of protease inhibitors, nor does it resemble the pattern obtained following endosomal acidification inhibition, in which generation of most of the L1 cleavage products required acidification, as the appearance of the lower bands was prevented by either NH_4Cl or bafilomycin A treatment (34).

Given this L1 processing defect, we evaluated whether it indicated a reduction in the efficiency of the separation of L2 from the capsid, which occurs prior to L2's egress from the LE/lysosome (22, 35). Therefore, we determined the amount of L1-associated L2 at 24 h postinfection in cells that were untreated or IFN-γ treated, using immunoprecipitation of samples with an anti-L1 polyclonal antiserum followed by Western blotting for the detection of L1 and L2 proteins (Fig. 3B). As expected, HPV16 infection of untreated cells (lane 4) resulted in some full-length L1 (upper) with little associated L2 (lower), although there was ample capsid-associated L2 in the input capsids (lane 2). As the L1-L2 dissociation occurs in a pH-dependent manner, the acidification inhibitor NH_4Cl was included as a positive control for L2 retention (lane 5). When the cells were treated

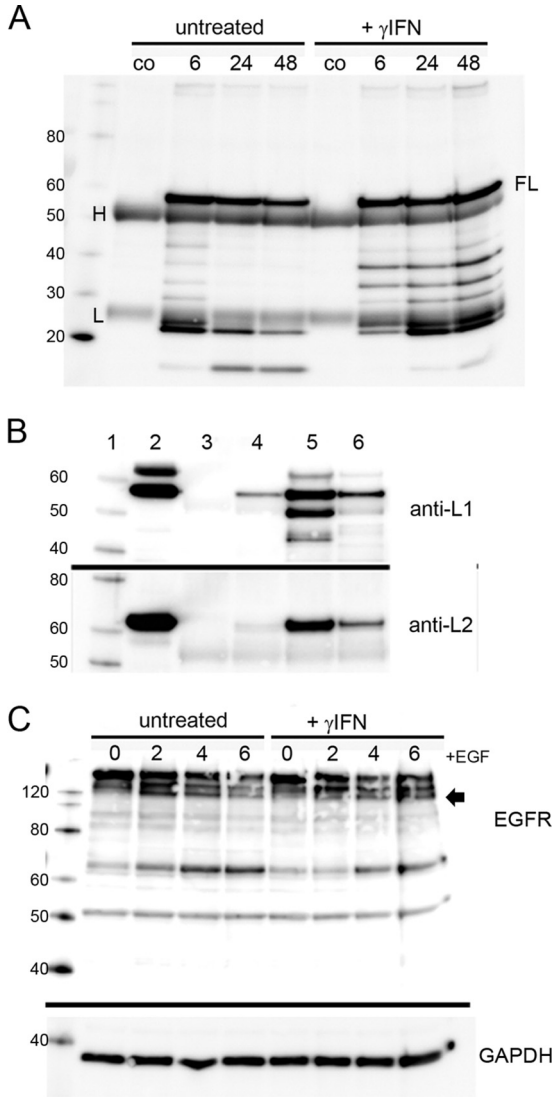

FIG 3 Intracellular processing in the presence of IFN-γ. (A) The intracellular processing of HPV16 L1 was examined by anti-L1 VLP immunoprecipitation using a rabbit polyclonal antiserum followed by Western blotting using a monoclonal antibody in both untreated and IFN-γ-treated HaCaT cells. Under the uninfected, cell-only conditions, indicated by "co," only the heavy- and light-chain antibody bands were evident (indicated as H and L). In the HPV16 PsV-infected cells the full-length, unprocessed L1 band (FL) was evident throughout the time course. Lower-molecular-mass products, migrating between 23 kDa and 45 kDa, were evident by 6 h under the untreated cell conditions. The 23-kDa band and an additional 15-kDa band were evident at the 24-h and 48-h time points. Under the IFN-γ-treated conditions, the intermediate-sized products did not resolve throughout the time course, and little accumulation of the 15-kDa band occurred. (B) The separation of the minor capsid protein, L2, from the major capsid protein, L1, was evaluated in untreated and IFN-γ-treated cells at 24 h postinfection. Uninfected cells (lane 3) or HPV16 PsV-infected cells (lane 4, untreated; lane 5, NH_4Cl treated; lane 6, IFN-γ treated) were immunoprecipitated with rabbit anti-L1 VLP antiserum, and the presence of the two capsid proteins was evaluated by Western blotting with mouse monoclonal antibodies (top, L1; bottom, L2). Lane 2 shows the migration of the input virion proteins. The lower band in lane 2 in the anti-L1 blot is the full-length L1 protein, and the upper band indicates cross-reaction of this antibody with the L2 protein. Most of the lower-molecular-mass L1 products shown in panel B were cropped out of this figure, but some of the weak, upper bands are evident in lanes 5 and 6. Following NH_4Cl treatment (lane 5), there was an increase in L1 and L1-associated L2. This was also evident, to a lesser degree, under the IFN-γ-treated condition (lane 6). (C) The intracellular processing of EGFR following EGF addition was examined in either untreated HaCaT cells or in IFN-γ-treated cells (18 h pretreatment) by Western blotting. The appearance of lower-molecular-mass forms of EGFR was similar under both conditions (arrow). The lower panel demonstrates equivalent protein concentrations by the comparison of GAPDH levels.

with IFN-γ (lane 6), there was an increase in the amount of L2 that remained associated with L1 (compare with lane 4), although it was less than that seen with NH_4Cl treatment (compare with lane 5). Collectively, the data indicate that HPV16 PsV processing/uncoating is incomplete in IFN-γ-treated HaCaT cells. The result does not phenotypically resemble that described for either protease inhibition or acidification inhibition.

There is substantial evidence that IFN-γ plays diverse roles during modulation of endocytic pathways (36) and results in the formation of enlarged endosomes in macrophages (37). Specific endocytically associated proteins induced by IFN-γ that we deemed to be potential effectors included GILT and Rab20. Rab20 functions in the maturation of phagocytic organelles, its expression was shown to be induced by IFN-γ in macrophages (38), and its overexpression induced the enlargement of the early endosomal and LE compartments (39). However, in HaCaT cells, we did not observe an increase in Rab20 expression following IFN-γ treatment (data not shown). GILT was a second appealing effector candidate; it is an IFN-γ-inducible thiol reductase that catalyzes the disulfide bond reduction of proteins, facilitating their further processing through cellular proteases (40, 41). As PV capsids are heavily disulfide bonded, reductive processes could be involved in intracellular uncoating. GILT is present in primary keratinocytes (42), but we found only low levels in HaCaT cells and no induction with IFN-γ (data not shown), although control cells, melanoma cell lines SK-MEL-2 and SK-MEL-28, showed strong induction, as expected (43). The increased expression of GILT in the melanoma cells did not correlate with a decrease in HPV16 PsV infection; infection of SK-MEL-28 was actually substantially increased following IFN-γ-treatment, whereas infection of SK-MEL-2 was decreased (data not shown). We conclude that neither Rab20 nor GILT is an effector of the IFN-γ-induced depression of HPV16 PsV infection.

We also determined if the effects observed for HPV16 capsid trafficking reflected a global cellular perturbation in endocytic trafficking induced by IFN-γ activation. To address this issue, we evaluated the entry of a cellular protein, transferrin receptor (TFR), and exogenous cargos with defined trafficking routes. TFR is internalized from the plasma membrane into the early endosome, with the majority recycling to the plasma membrane and a subset continuing into lysosomes, where it is degraded (44, 45). We examined the TFR distribution following overnight treatment with IFN-γ and compared the steady-state receptor distribution to that of untreated cells (Fig. 4A and B). IFN-γ treatment did not induce a distinctive difference in the distribution of TFR, although its staining intensity was clearly increased, probably indicating a minor kinetic perturbation. We also tracked the internalization of the cargo protein, epidermal growth factor (EGF), which, in association with its receptor (EGFR), traffics from the plasma membrane to the late endosomal compartment via early endosomes. EGF is degraded following internalization, whereas EGFR can either be recycled back to the cell surface or degraded in lysosomes (46–48). We first examined the colocalization of EGF with the early endosomal marker EEA1 at both 30 min and 120 min following the addition of Alexa 488-coupled EGF in the presence or absence of overnight treatment with IFN-γ prior to cargo addition (Fig. 4C to F). Unsurprisingly, partial colocalization of EGF with EEA1 was evident in the untreated cells at 30 min (Fig. 4C). At this early time point in the IFN-γ-treated cells, this colocalization was not prevented and was possibly slightly enhanced (Fig. 4D). A more distinct difference was observed at the later time point. In the untreated cells (Fig. 4E), EGF was no longer localized to early endosomes, and the fluorescent signal was reduced, presumably due to degradation. The IFN-γ-treated cells also demonstrated a passage of EGF out of the early endosomes (Fig. 4F); however, the intensity of the EGF staining was not greatly reduced compared to the earlier time point. These results indicate that EGF trafficking through the late endosomal compartment or lysosomal degradation are affected by IFN-γ treatment of HaCaT cells. We also evaluated the impact of IFN-γ treatment on the degradation of EGFR following addition of EGF (Fig. 3C). However, the appearance of lower-molecular-weight forms of EGFR, indicating receptor processing, was similar in the presence or absence of IFN-γ, although a possible slight delay in degradation following IFN-γ treatment may be seen

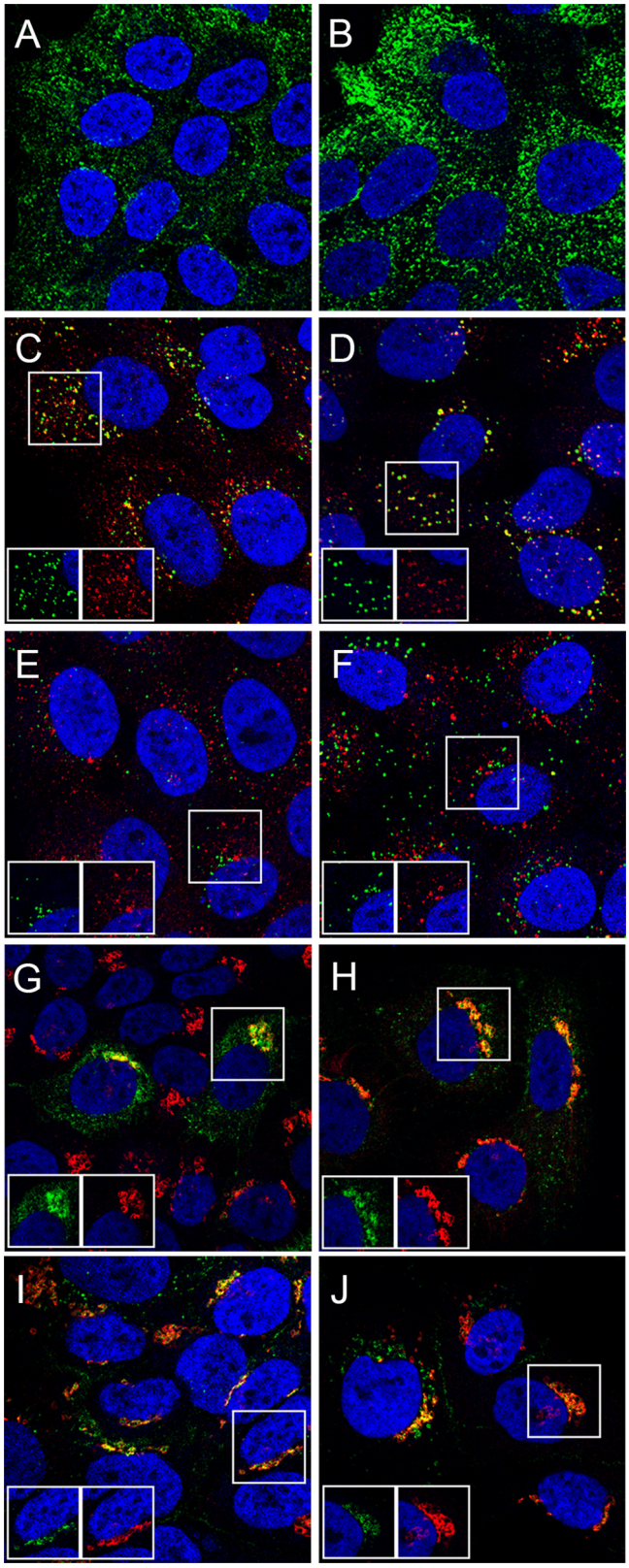

FIG 4 Effect of IFN-γ treatment on protein trafficking. HaCaT cells were left untreated or were treated with IFN-γ for 18 h. The untreated conditions are shown in the left column and the IFN-γ-treated conditions are in the right column. The steady-state distribution of the transferrin receptor (TFR) was examined and is shown in panel A (untreated) and panel B (treated). The delivery of Alexa 488-coupled epidermal growth factor (EGF; green channel) to early endosomes, as indicated by anti-EEA1 staining (red

(Continued on next page)

at the 2-h time point, as indicated by the less intense lower band (Fig. 3C, arrow). Thus, IFN-γ does not cause a dramatic change in EGFR processing in HaCaT cells.

We examined two cargo proteins, cholera toxin B (CTXB) and ricin, that have been reported to utilize the retromer complex to access to the *trans*-Golgi network (TGN) from early endosomes (49–51). The localization of Alexa 488-coupled cholera toxin B (CTXB-488) was evaluated in cells that were treated overnight with IFN-γ or left untreated. CTXB-488 was allowed to internalize for 30 min to allow substantial time to traffic into the TGN. It was clear that the IFN-γ treatment had no effect on the ability of CTXB to enter the Golgi complex, as indicated by colocalization with giantin (compare Fig. 4G [untreated] to H [IFN-γ treated]). Likewise, we evaluated the trafficking of Alexa 488-coupled ricin under these conditions. There was also no effect on Golgi localization of ricin following a 30-min incubation (compare Fig. 4I [untreated] to J [IFN-γ treated]). Thus, in HaCaT cells, retromer-dependent trafficking from the early endosome to the Golgi complex is not disrupted by IFN-γ treatment.

Sensitivity of other cell lines. All of the above-described analyses, except for the GILT control experiments with the melanoma cell lines, were performed in HaCaT cells, a normal human skin-derived keratinocyte cell line. Therefore, we determined if the observed effect could be observed in additional cell lines relevant for HPV studies (Fig. 5A). HPV16 PsV infection of the 293TT cell line, which is an adenovirus-transformed human cell line used for HPV PsV propagation but is not considered a good system in which to study HPV entry, was completely insensitive to IFN-γ treatment. HPV16 PsV infection of HeLa cells, which are derived from an HPV18-positive cervical adenocarcinoma, showed an intermediate sensitivity to IFN-γ treatment, with a maximum inhibition of less than 70%. Ect1 E6/E7, a cell line derived from normal human ectocervical epithelium that had been immortalized by expression of HPV16 E6/E7, showed complete inhibition of HPV16 PsV infection following IFN-γ treatment. However, this line was less sensitive than HaCaT cells, with the inhibition dropping off sharply in Ect1 E6/E7 at concentrations progressively lower than 2 ng/ml, in contrast to HaCaT. We also examined the sensitivity of HPV16 PsV infection of a murine keratinocyte cell line, S1, to murine IFN-γ treatment. This cell line demonstrated low sensitivity to the treatment, with a maximum inhibition of 40%. We verified that all of these cell lines could respond to IFN-γ by confirming the appearance of the phosphorylated form of STAT1 in response to IFN-γ treatment (Fig. 5B, lower). The upper portion of Fig. 5B shows the detection of endogenous STAT1. Therefore, all cell lines were clearly responsive to IFN-γ despite the observed differences of this treatment on HPV16 PsV infection. Importantly, it is clear that the IFN-γ phenotype is not confined to the HaCaT cell line.

HPV genera are differentially affected by IFN-γ treatment. To see if the IFN-γ sensitivity of HPV16 PsV extended to other HPV types, we compared the infection of HaCaT cells, either untreated or treated overnight with IFN-γ, by 17 additional HPV PsV types, including alpha and beta genus members. HPV16 is a genus alpha, species 9 member, and we analyzed four additional species alpha 9 members: HPV31, HPV33, HPV52, and HPV58 (Fig. 6A). Infection with three of the alpha 9 members was strongly inhibited by IFN-γ treatment (HPV31, HPV52, and HPV58), but HPV33 showed only an intermediate sensitivity, with approximately 50% maximum inhibition. The representatives of alpha 8, HPV40, and alpha 11, HPV73, also showed strong inhibition of infection (Fig. 6B), whereas two alpha 10 members, HPV6 and HPV11, were only weakly

FIG 4 Legend (Continued)
channel), was examined at two time points following EGF addition; the 30-min time point is shown in panels C (untreated) and D (treated), and the 2-h time point is shown in panels E (untreated) and F (treated). Note that the slightly increased EGF signal at the 2-h time point does not colocalize with EEA1. For each panel a selected region is shown as a split image. (G to J) The Golgi delivery of the retromer-dependent cargoes, Alexa 488-coupled cholera toxin B (CTXB-488) and FITC-coupled ricin (green channel), was determined by colocalization with giantin (red channel). Delivery of both reagents was examined at 30 min postaddition. For each panel, a selected region is shown as a split image within the panels; untreated cells are shown in panel G (CTXB) and panel I (ricin), and IFN-γ-treated cells are shown in panel H (CTXB) and panel J (ricin).

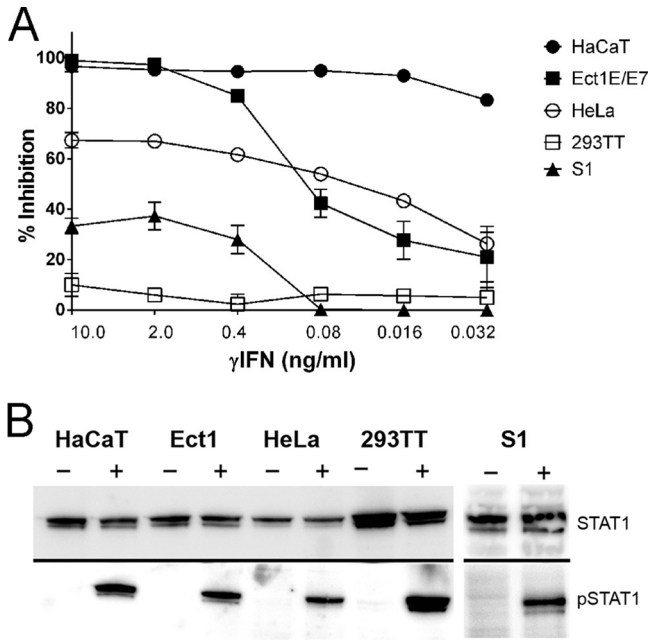

FIG 5 Evaluation of IFN-γ treatment of other cell lines. (A) To determine the IFN-γ sensitivity of HPV16 PsV infection in additional cell lines, we pretreated a panel of cell lines with the indicated concentration for 18 h prior to HPV16 PsV addition. GFP-positive cells were determined at 72 h postinfection and normalized to the untreated, infected population. The S1 cell line was treated with murine IFN-γ. Triplicate infections were analyzed for all experiments. (B) The ability of these cell lines to respond to IFN-γ treatment was determined by Western blotting of the endogenous form of STAT1 (upper) and the appearance of the tyrosine 701-phosphorylated form of STAT1 (lower). The inclusion of IFN-γ is indicated by the plus sign above the appropriate lane. Note that all cell lines have an intact IFN-γ activation capacity.

inhibited. We examined five members of the alpha 7 species, HPV18, HPV39, HPV59, HPV45, and HPV68 (Fig. 6C), and observed approximately 80% inhibition of HPV18 infection, but the other species members were not strongly affected by IFN-γ treatment. HPV39 and HPV45 were particularly insensitive. Additionally, an alpha 5 representative, HPV26, was poorly inhibited. We also determined the inhibition profile of three genus beta members: species beta 1 members HPV5 and HPV8 and the beta 2-type HPV38. Infection of all three types was strongly inhibited by IFN-γ treatment (Fig. 6D). We also examined the sensitivity of three animal PV types: BPV1, CRPV, and MusPV1. Infection of BPV1 and CRPV was strongly inhibited (more than 80% inhibition), whereas inhibition of MusPV1 was intermediate (approximately 40% maximum inhibition) (data not shown). Thus, the sensitivity to IFN-γ is not limited to HPV16, to alpha 9 species members, or to human PV types. However, the relative insensitivity of four of the five tested alpha 7 types is especially intriguing. These data also reinforce the conclusion that IFN-γ treatment does not globally inhibit endosomal trafficking in HaCaT cells, because such an effect would have been predicted to affect all PV types equally, as no studies have proven the utilization of distinct entry pathways for different HPV types (52–54).

IFN-γ sensitivity correlates with L2 type. Given the heterogeneity of the various HPV types to inhibition by IFN-γ treatment, we reasoned that it might be possible to determine whether the sensitivity of a given HPV type was attributable to its L1 or L2 protein through the analysis of hybrid L1/L2 infectious PsV whose capsid proteins were derived from HPV types that differ in their sensitivity to IFN-γ. It is known that, for some PV types, it is possible to exchange the two capsid proteins between two different types and obtain intact, assembled particles. For instance, HPV11 L1 was found to form complexes with L2 proteins from a variety of other HPV types, including non-alpha 10 types, and even with the animal type COPV1 (55). We found that infectious PsV can be

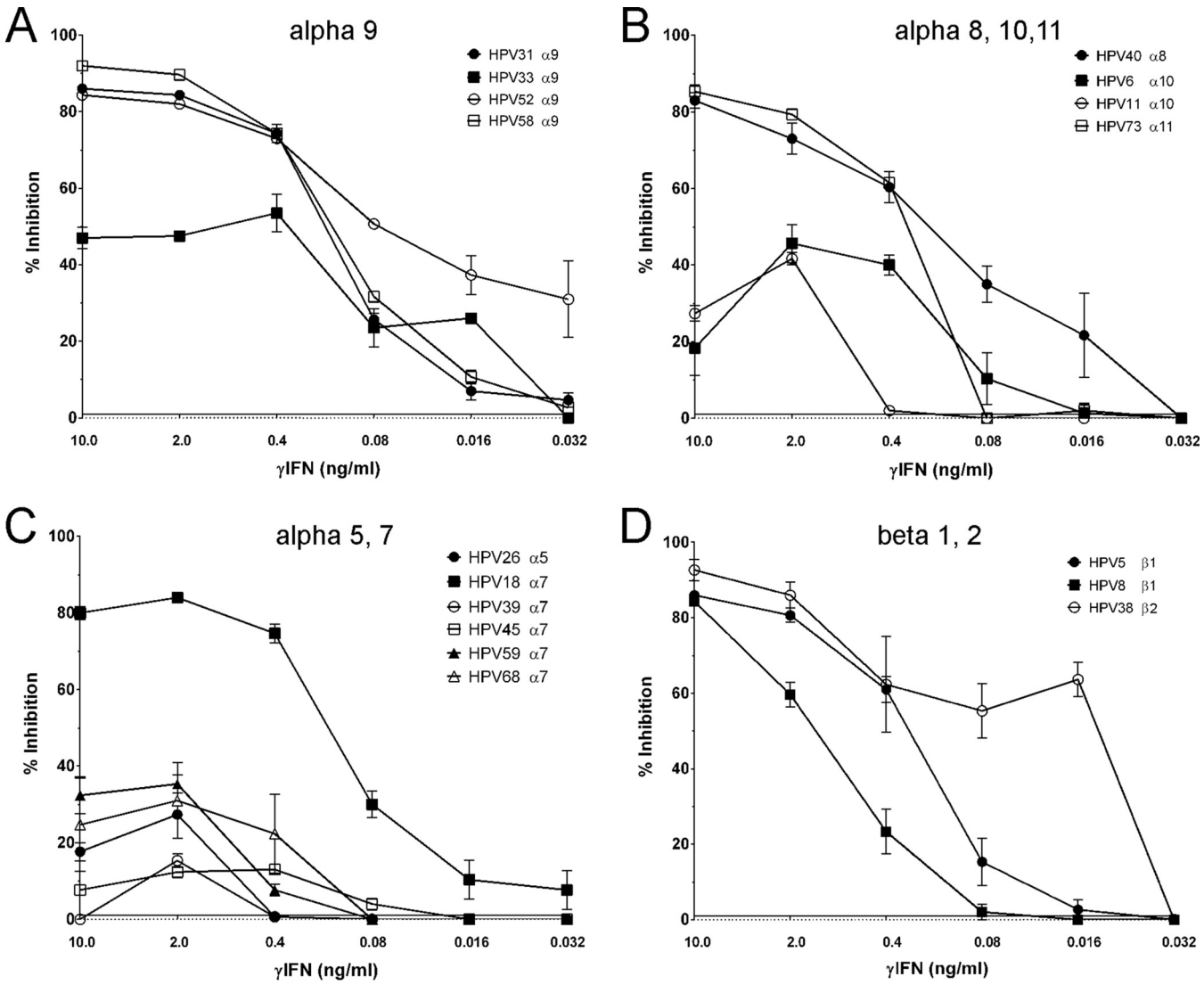

FIG 6 Susceptibility of other HPV types to IFN-γ treatment. To determine if other HPV types also showed a sensitivity to IFN-γ treatment, we examined the infection of a panel of HPV PsV types on HaCaT cells. All PsV types were initially titrated to determine the PsV amount to generate 15 to 30% infected cells. This amount was then used to infect untreated cells and cells that had been treated with a titration series of IFN-γ. The percentage of inhibition was determined by normalizing to the untreated control infection. The species groupings are indicated above each panel and next to the HPV type indicated. (A) Alpha 9 species members; (B) alpha 8, 10, and 11; (C) alpha 5 and 7; (D) beta 1 and 2 members. Triplicate infections were analyzed for all experiments.

produced from some, but not all, capsid protein combinations (Fig. 7A and unpublished data). To determine if the disparate IFN-γ effects observed for the various HPV types could be attributed to either of the individual capsid proteins, we produced infectious hybrid particles between HPV45 L1 as the type insensitive to IFN-γ treatment and HPV16 L2 as the sensitive type (termed HPV45/16). The inverse combination (HPV16/45) did not produce infectious particles, although coassembly was robust (data not shown). HPV45/16 PsV infection was inhibited by IFN-γ treatment, whereas the IFN-γ responses of HPV16 L1/L2 and HPV45 L1/L2 were sensitive and insensitive, respectively, as expected (Fig. 7A). The IFN-γ-sensitive capsid protein in the hybrid PsV was derived from HPV16 L2, and this result suggests that the L2 protein determines the IFN-γ sensitivity phenotype of the HPV. Given that HPV16/45 PsV did not result in infectious particles, we produced hybrid PsV from a different combination of PV capsid proteins to test the hypothesis that IFN-γ sensitivity maps to the L2 protein. Hybrid particles from HPV45 and HPV18, two alpha 7 types that displayed opposite phenotypes in response to treatment, were assembled. Fortuitously, in this instance both hybrid

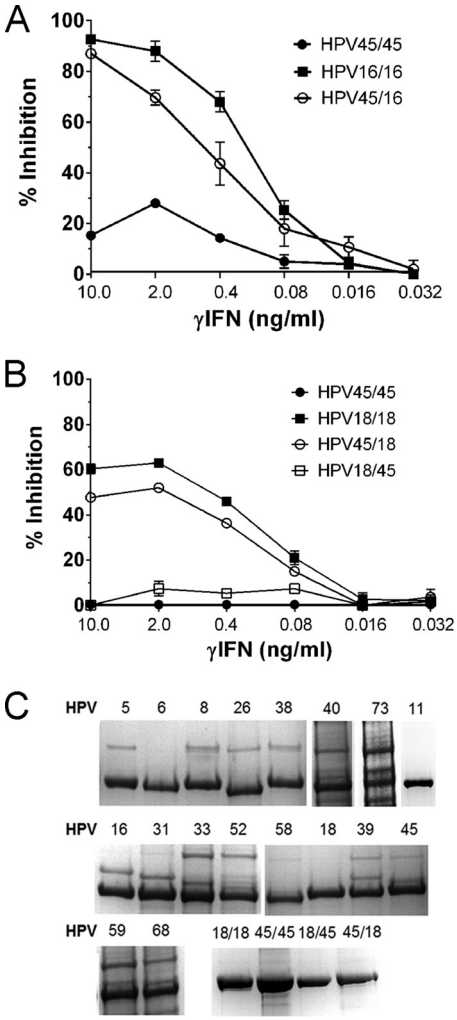

FIG 7 HPV type of the L2 protein confers IFN-γ response phenotype. Hybrid HPV PsVs were assembled and infectivity was confirmed by titration on HaCaT cells. The PsV amount to confer 15 to 35% infection was then used to evaluate the sensitivity to IFN-γ. (A) Both HPV16 and HPV45 displayed their previously demonstrated infection phenotype following IFN-γ treatment. The hybrid PsV that contained the HPV45 L1 protein and the HPV16 L2 protein shared the sensitivity of the HPV16 PsV to IFN-γ treatment. (B) Hybrid PsV were assembled to contain HPV45 L1 and HPV18 L2 and the inverse shuffle, HPV18 L1 and HPV45 L2. The former capsid combination was sensitive to IFN-γ treatment, like the HPV18/18 PsV. The latter PsV, with HPV45 L2, was not sensitive to IFN-γ treatment, resembling the HPV45/45 PsV. (C) The capsid composition and purity were determined for each PsV type. Purified particles were examined by Coomassie G-250 staining. The dominant band in each type is the L1 protein, and the more slowly migrating band evident in some types is the L2 protein. HPV18 and HPV45 PsV preparations that were generated with the bicistronic expression plasmid and the two separate L1 and L2 expression plasmids are both shown.

combinations resulted in infectious PsV. The results with these hybrids confirmed that L2 mediates the sensitivity to IFN-γ, as the HPV45/18 hybrid, whose L2 is from the IFN-γ-sensitive HPV18, was inhibited by IFN-γ, while the HPV18/45 hybrid, whose L2 is from the IFN-γ-insensitive HPV45, was resistant to IFN-γ (Fig. 7B).

Different HPV PsV types can have different L1/L2 ratios and also exhibit various particle-to-infectivity ratios, and the two can only be partially correlated (52). To confirm that the differential effects of IFN-γ that we observed were not attributable to a trivial explanation, such as the level of L2 incorporation or purity of particle preparation, all PsV were analyzed by SDS-PAGE and Coomassie G-250 staining (Fig. 7C). Although there was a range of incorporated L2 levels among these preparations, with L2 being undetectable in some instances, there was no obvious correlation with either L2 incorporation or PsV purity and IFN-γ sensitivity. As an example, an L2 band is clearly

evident for HPV26, HPV39, HPV59, and HPV68, all IFN-γ-insensitive types. L2 is equally obvious for HPV5, HPV8, HPV38, HPV40, HPV52, and HPV73, IFN-γ-sensitive types.

DISCUSSION

The IFN family plays a pivotal role in the control of many viral infections and in shaping the subsequent adaptive immune response. Their actions are mediated through signaling pathways triggered by the engagement of receptors that activate the expression of IFN-stimulated genes (ISGs). Each IFN induces a distinct ISG profile that includes both shared and unique members (56, 57). These ISG proteins can exert, among numerous other activities, antiviral actions that can target vulnerabilities at all stages of the viral life cycle, including entry, transcription, translation, genome replication, assembly, and egress (reviewed in reference 58), although the described effects of most reports have concluded that the inhibition is largely at the level of viral transcription and translation, including studies on the structurally related polyomaviruses (59, 60). The identified effector molecules in these studies include RNA-dependent protein kinase (PKR), adenosine deaminase (ADAR), guanylate-binding proteins (GBP1 and GBP2), and nitric oxide synthetase (NOS), although in other instances the observed effects are unascribed (61–67).

We initiated this study to evaluate the entry step at which type I IFNs, both IFN-α and IFN-β, inhibited HPV16 PsV infection of HaCaT cells, which had been described by Warren et al. (6). However, we were unable to observe an effect of type I IFN on HPV16 PsV infection, despite repeated attempts with reagents from various sources, including the same source, treatment time, and concentration utilized in the previous study. The only clear distinction between the protocols is that we utilized a GFP reporter system which allows determination of the number of infected cells after gating on only living cells, whereas the previous study used a luciferase reporter. In that assay system, the luciferase signal is obtained from the lysate of the entire cell population, which would include cells adversely affected by the treatment. This difference could explain the disparate results. Indeed, when we performed an inhibition assay using HPV16 PsV containing a Dual Luciferase/GFP reporter plasmid, we observed inhibition in the luciferase assay, comparable to that previously reported, but not in the GFP flow-cytometric assay (unpublished data).

Given that we have evaluated PsV, our results do not address the possibility that type I IFNs influence later aspects of the viral life cycle, as would be predicted from the observation that the viral oncoproteins actively inhibit IFN-mediated cellular responses (68–71), and numerous studies have demonstrated the efficacy of type I interferon in the clearance of episomal HPV genomes (72, 73).

In contrast to type I IFNs, we observed a dramatic abrogation of HPV16 PsV infection following IFN-γ treatment, which had not been examined previously. This inhibition was mediated through the canonical JAK/STAT pathway, although type I IFN treatment also can induce this pathway in HaCaT cells (74 and data not shown); therefore, the critical induction downstream of this activation is not shared between these treatments. Interestingly, the inhibition of infection occurred at the level of virus entry and trafficking, prior to nuclear delivery of the viral genome. Based on our microscopic and biochemical analysis, endosomal capsid processing was affected, proteolytic digestion of L1 was incomplete, and L2 was not resolved from the capsid complex as typically occurs during PV uncoating. This processing block did not mimic that observed following neutralization of the endosomes or inhibition of essential proteases, as previously reported (34).

A parallel IFN-γ effect was reported for influenza A virus, where it was found that the incoming viral particles were sequestered in an expanded LE compartment and viral fusion was prevented. However, this effect was attributable to induction of IFITM3 (75), which has been convincingly demonstrated to have no effect on HPV16 PsV infection (6); therefore, this mechanism is unlikely to be mediating the effects described here. Other IFN-γ-induced effector molecules that are known to affect the endosomal compartment include Rab20 and GILT (38–41), but our analyses lead us to conclude

that neither protein makes a major contribution to the inhibition of HPV16 PsV infection.

Although the normal endosomal processing of HPV16 capsids was prevented in the IFN-γ-treated cells, we demonstrated by both biochemical and microscopic methods that vesicular processing was not globally affected. Therefore, it is unlikely that our observations reflect a general inhibition of endosomal degradation or severe cellular perturbation. Further supporting this conclusion are the data that some HPV types were impervious to IFN-γ activation, and distinct entry pathway usage for various PVs has not been demonstrated (53, 54). No HPV PsV types have been described to be resistant to either furin inhibition or gamma secretase inhibition, which reflect both extracellular and intracellular processing requirements, although differences in cell surface interactions have been described (13, 16, 52). The effect of IFN-γ treatment on endosomal pH and protein processing has been well documented in macrophages. These studies have concluded that IFN-γ treatment does not result in less efficient acidification or change the proteolytic activity of the lysosomal/phagosomal compartments (76–78). However, as these studies were all performed in macrophages, we could not assume that IFN-γ activation of HaCaT cells did not affect endosomal pH. It has been well established that PVs require passage through the low-pH environment of the LE for infection (13). However, as we observed differences among HPV types in their sensitivity to IFN-γ, we wanted to ensure that this heterogeneity was not associated with subtle differences in pH dependence. We performed a titration of both bafilomycin A and NH_4Cl, which indicated that all members of a panel of sensitive and resistant types were equally sensitive to the pharmacologically induced higher pH (data not shown).

One of the interesting facets of our study is the observation that PsV inhibition is mediated through the L2 protein. As previously mentioned, L2 segregates with the viral DNA from L1 during endocytosis. This segregation is pH dependent and is mediated, at least in part, by the action of cyclophilins (35). Our biochemical and fluorescent analyses indicate that IFN-γ treatment prevents this dissociation event. To evaluate if IFN-γ interferes with the action of cyclophilins, we assessed the susceptibility of a panel of PsV, including those most sensitive and most insensitive to IFN-γ, to cyclosporine (CSA), a cyclophilin inhibitor. We found no correlation between these profiles; as a specific example, HPV45, a type relatively impervious to IFN-γ, was inhibited with CSA to the same extent as HPV16 (data not shown).

As shown, some genera seem to be resistant to treatment. The sensitivity phenotype is roughly correlative with genotype, but there are notable exceptions, e.g., HPV18 is the sole sensitive alpha 7 member. This observation indicates that aspects of the uncoating process, at the level of L2/genome dissociation from L1, must differ across the HPV lineage or at least among HPV types. Type-specific differences in uncoating have not been previously described. Identification of the critical ISG or interferon-regulated gene (IRG), as the observed effect could also be due to downregulation of an essential protein, will be instrumental in understanding this aspect of HPV intracellular trafficking. This information could explain why some HPV types are resistant and possibly indicate how the various types differ in the critical step of L2/DNA segregation from the endocytosed capsid.

MATERIALS AND METHODS

Reagents. The following sources for IFNs were used: recombinant human gamma interferon (>98% purity; cyt-206; ProSpec), recombinant mouse gamma interferon (>95% purity; cyt-358; ProSpec), recombinant human alpha interferon 2b (>98% purity; cyt-205; ProSpec), recombinant human alpha interferon 2a (>97% purity; cyt-204; ProSpec), and recombinant human lambda interferon 1 (>98% purity; PeproTech 300-02L; ProSpec). Additionally, human leukocyte IFN-α (NR-3078) and human recombinant IFN-β (NR-3085) were obtained through BEI Resources, NIAID, NIH (purity levels not given). The inhibitors PF-573228 (S2013; >99% purity), ruxolitinib (S1378; >99% purity), U1026 (S1102; >99% purity), and CEP-33779 (S2806; >99% purity) were obtained from Selleck Chemicals. The inhibitors imidazole-oxindole (C16) (I9785; >98% purity) and stattic (S7947; >98% purity) were obtained from Sigma-Aldrich. Fluorescein-labeled *Ricinus communis* agglutinin II (ricin) (FL-1091) was purchased from Vector Laboratories. Cholera toxin subunit B conjugated to Alexa Fluor 488 (C34775) and Alexa Fluor 488-conjugated epidermal growth factor (EGF) (E-13345) were purchased from Invitrogen.

Cell lines. The human keratinocyte cell line HaCaT, originally from Norbert Fusenig (79), and the HeLa and 293TT (11) cell lines were cultured in Dulbecco's modified Eagle's medium (DMEM) supplemented with 10% fetal bovine serum (FBS) and penicillin-streptomycin (P/S). The murine keratinocyte cell line S1 was a kind gift from Stuart Yuspa (NCI, NIH) (80). The epithelial ectocervical cell line Ect1 E6/E7 was obtained from ATCC (CRL-2614). Both of these cell lines were also cultivated in DMEM with 10% FBS and P/S. SK-MEL-2 and SK-MEL-28 are part of the NCI-60 tumor cell line panel and were obtained from the Developmental Therapeutics Program at the National Cancer Institute, NIH (Frederick, MD).

Antibodies. The rabbit polyclonal antisera recognizing HPV16 and HPV45 capsids were previously described (81, 82), as were the anti-L2 monoclonal antibodies K1L2 (L2 amino acids 64 to 81), used for immunofluorescent detection, and K5L2 (47–51, 53–67), used for Western blot detection, both kind gifts from Martin Müller (DKFZ, Heidelberg) (83). The anti-LAMP-1 monoclonal antibody (H4A3), developed by August et al., was obtained from the Developmental Studies Hybridoma Bank developed under the auspices of NICHD and maintained by the Department of Biological Sciences at the University of Iowa (84). All other antibodies were obtained from commercial sources. Camvir-1 antibody (Abcam) was used to detect HPV16 L1 on Western blots. Rabbit anti-giantin was obtained from BioLegend (924302). Mouse anti-TFR was purchased from Zymed (13-6800). Rabbit anti-glyceraldehyde-3-phosphate dehydrogenase (GAPDH) (14C10), rabbit anti-ERK1/2 (9102S), rabbit anti-pERK1/2 (9101S), rabbit anti-STAT3 (12640S), and rabbit anti-pSTAT3 (9145S) were from Cell Signaling Technology. The antibodies against FAK (610087) and pFAK (611723) were from Becton Dickinson. The antibodies recognizing EGFR (sc-03), STAT1 (sc-346), and tyrosine 701-phosphorylated STAT1 (sc-13648) all were purchased from Santa Cruz Biotechnology, Incorporated.

Pseudovirus production. PsV preparations were produced according to the improved, standard production protocol published on the laboratory website (http://home.ccr.cancer.gov/lco/plasmids.asp) (85). Briefly, 293TT cells were transfected with either a bicistronic plasmid encoding the PV L1 and L2 proteins or two plasmids separately encoding the capsid proteins, together with a reporter gene plasmid encoding GFP (pfwB). Purity and L1 content were assessed following protein staining of SDS-PAGE gels with SimplyBlue SafeStain, a Coomassie G-250 stain (Invitrogen). For infection, PsV were used at a concentration titrated to yield 15 to 30% GFP positivity. The nanogram amount (based on L1 content) needed to obtain this infectivity varies according to PsV type and is noted after the type. The plasmids used for the various types were HPV16 (2 ng), p16sheLL; HPV5 (40 ng), p5shell; HPV6 (40 ng), p6sheLL; HPV11 (50 ng), p11L1w and p11L2w; HPV18 (2 ng), p18sheLL; HPV31 (10 ng), p31sheLL; HPV45 (1 ng), p45sheLL; HPV52 (65 ng), p52sheLL; and HPV58 (4 ng), p58sheLL. For the additional types, i.e., HPV8 (80 ng), HPV26 (2 ng), HPV33 (3 ng), HPV38 (100 ng), HPV39 (2 ng), HPV40 (40 ng), HPV59 (5 ng), HPV68 (4 ng), and HPV73 (915 ng), we used the corresponding pVITRO bicistronic expression plasmid described by Kwak et al. (52), kind gifts from Richard Roden (Johns Hopkins University). For assembly of the hybrid PsV particles, HPV45/16 (15 ng), HPV18/45 (3 ng), and HPV45/18 (2 ng) were used with the following plasmids: HPV16 L1, p16L1h; HPV16L2, p16L2h (p16L1h and p16L2h both were generated in our laboratory); HPV45L1, HPV45L1HD; HPV45L2, HPV45L2HD; HPV18L1, HPV18L1HD; and HPV18L2, HPV18L2HD. These were all kind gifts from Martin Müller (DKFZ). Where indicated, PsV were assembled in the presence of 50 μM 5-ethynyl-2′-deoxyuridine (EdU) supplemented to the growth medium at 6 h posttransfection as previously described (22). Assembled particles were released by detergent lysis, matured in the presence of 25 mM ammonium sulfate, and purified by ultracentrifugation through an OptiPrep step gradient (85). For control experiments, HPV16 PsV packaging pcLucf, which encodes both GFP and firefly luciferase, was produced. Quantification of luciferase activity was performed with the Britelite plus kit (6066761; PerkinElmer) according to the manufacturer's directions.

Pseudovirus infection. To assess infection, PsV dilutions were added to HaCaT cells that had been grown overnight at a plating density of 8×10^3 cells per well in 96-well plates. The percentage of GFP-transduced cells was determined by flow-cytometric analysis (BD FACSCalibur) after a 48- to 72-h infection period. Prior to analysis, cells were dislodged with 50 μl 0.25% trypsin. Following this, 150 μl of fluorescence-activated cell sorter (FACS) buffer (phosphate-buffered saline [PBS] containing 2% FBS and 0.1% sodium azide) was added to each well, and cells were processed on a Becton Dickinson FACSCanto II cytometer equipped with a high-throughput plate reader. Live cells were selectively gated by forward scatter/side scatter considerations. Addition of IFN was performed 18 h prior to initiation of PsV infection unless otherwise noted. Biochemical inhibitors of potential IFN activation were added immediately prior to IFN addition. All flow cytometry experiments were performed in triplicate and repeated a minimum of three times.

Immunofluorescent staining. Cells were seeded onto glass no. 01 coverslips in a 24-well plate at a density of 8×10^4/well and cultured overnight. For evaluation of internalized PsV, 20 ng of PsV was added to each well and allowed to bind and internalize for 24 h. Following this incubation, cells were fixed in ice-cold ethanol containing 15 mM glycine and processed for immunofluorescent staining. Detection of EdU-labeled pseudogenomes was performed with the Click-It 488 Alexa Fluor EdU imaging kit (Invitrogen) as previously described (22). For visualization of other cargo, incubation was performed for the time period indicated. EGF-488 was used at a concentration of 1 μg/ml, CTXB-488 was used at 5 μg/ml, and ricin-fluorescein isothiocyanate (FITC) was used at 10 μg/ml. Following these incubations, the cells were fixed in 2% paraformaldehyde in PBS for 20 min at room temperature, at which time the coverslips were washed in PBS containing 200 mM glycine and processed for immunofluorescent detection of marker proteins, as previously described (86). Stained coverslips were mounted by inversion onto 4′,6-diamidino-2-phenylindole (DAPI)-containing solution (Prolong Gold; Molecular Probes). All images were acquired with a Zeiss 780 confocal system interfaced with a Zeiss Axiovert 100M microscope. Images were collated with Adobe Photoshop software. The insets in Fig. 2A and B show

surface-rendered images of Z-stack images that were processed with Imaris software. Lysosomal diameters were measured with the Imaris software following surface rendering. Significance was determined using Welch's unequal variance *t* test. The colocalization histograms shown in Fig. 2C to F were created by line profile analysis in Zen software (Zeiss). The pixel values were exported to GraphPad Prism 7.

PsV processing. To examine the intracellular processing of HPV16 PsV, 4×10^5 HaCaT cells/well were plated in 6-well plates overnight and then treated with 2 ng/ml IFN-γ prior to incubation with PsV. Nine hundred nanograms of PsV, based on L1 protein amount, was added per well and incubated for the indicated time. Following this, cells were removed with 0.25% trypsin, washed twice with PBS, and lysed in immunoprecipitation buffer (50 mM Tris-HCl, pH 8.0, 100 mM NaCl, 50 mM NaF, 0.5% NP-40, and 0.1% SDS containing Complete protease inhibitor cocktail [Roche]) for 20 min on ice. Cellular debris was removed by centrifugation. Clarified lysates were incubated with rabbit anti-HPV16 L1 VLP antiserum and protein A/G Sepharose (Pierce) overnight in the cold with rocking. Immunoprecipitated complexes were collected by centrifugation and washed 4 times in IP buffer. The remaining complexes were boiled in SDS-PAGE sample buffer, resolved on a 4 to 12% NuPage gel (Invitrogen), and transferred to an Immobilon membrane (Millipore). HPV16 L1 was detected with the Camvir1 antibody. For determination of L1-associated L2 protein, the above-described procedure was followed. If indicated, the addition of NH_4Cl was coincident with the addition of PsV to a final concentration of 20 mM. L2 was detected by Western blotting with the K5L2 antibody (47–51, 53–67).

EGFR processing. To evaluate the cellular processing of EGFR, 4×10^5 HaCaT cells, plated in 12-well plates, were either left untreated or were IFN-γ treated (2 ng/ml) overnight. Cells were then incubated with 10 mg/ml cycloheximide for 30 min prior to addition of 100 ng of EGF and incubated for the indicated times. Cells were lysed directly in SDS-PAGE sample buffer (500 μl) and boiled, and 35 μl was loaded on a 4 to 12% NuPage gel for Western blot analysis.

Cell activation. The ability of IFN-γ to activate the phosphorylation of STAT1 was determined by Western blotting. A total of 4×10^5 cells/well was plated in a six-well plate and cultured overnight. The cells were either left untreated or were treated with 100 ng/ml of the indicated IFN for 60 min. Cells were lysed directly in SDS-PAGE sample buffer (500 μl) and boiled, and 35 μl was loaded on a 4 to 12% NuPage gel for Western blot analysis. All inhibitors were confirmed to be efficacious in HaCaT cells by evaluation of the phosphorylation status of an appropriate protein as detailed in the figure legends. For evaluating the activity of stattic, interleukin-6 (20 ng/ml) was added to the cells 15 min after the addition of stattic.

ACKNOWLEDGMENTS

We thank Richard Roden and Joshua Wang from Johns Hopkins University and Martin Müller from DKFZ-Heidelberg for the generous sharing of reagents. We also thank the CCR-NCI-NIH confocal core facility for access to their facilities.

Research was supported by the Intramural Research Program of the National Institutes of Health, National Cancer Institute, Center for Cancer Research.

REFERENCES

1. Plummer M, de Martel C, Vignat J, Ferlay J, Bray F, Franceschi S. 2016. Global burden of cancers attributable to infections in 2012: a synthetic analysis. Lancet Glob Health 4:e609–616. https://doi.org/10.1016/S2214-109X(16)30143-7.
2. Howley PM, Schiller JT, Lowy DR. 2013. Papillomaviruses, p 1662–1703. *In* Knipe DM, Howley PM, Cohen JI, Griffin DE, Lamb RA, Martin MA, Racaniello VR, Roizman B (ed), Fields virology, 6th ed. Lippincott Williams & Wilkins, Philadelphia, PA.
3. Stanley M. 2010. HPV–immune response to infection and vaccination. Infect Agents Cancer 5:19. https://doi.org/10.1186/1750-9378-5-19.
4. Frazer IH. 2009. Interaction of human papillomaviruses with the host immune system: a well evolved relationship. Virology 384:410–414. https://doi.org/10.1016/j.virol.2008.10.004.
5. Vedham V, Divi RL, Starks VL, Verma M. 2014. Multiple infections and cancer: implications in epidemiology. Technol Cancer Res Treat 13:177–194.
6. Warren CJ, Griffin LM, Little AS, Huang IC, Farzan M, Pyeon D. 2014. The antiviral restriction factors IFITM1, 2 and 3 do not inhibit infection of human papillomavirus, cytomegalovirus and adenovirus. PLoS One 9:e96579. https://doi.org/10.1371/journal.pone.0096579.
7. Isaacs A, Lindenmann J. 1957. Virus interference. I. The interferon. Proc R Soc Lond B Biol Sci 147:258–267. https://doi.org/10.1098/rspb.1957.0048.
8. Stark GR, Kerr IM, Williams BR, Silverman RH, Schreiber RD. 1998. How cells respond to interferons. Annu Rev Biochem 67:227–264. https://doi.org/10.1146/annurev.biochem.67.1.227.
9. de Weerd NA, Nguyen T. 2012. The interferons and their receptors–distribution and regulation. Immunol Cell Biol 90:483–491. https://doi.org/10.1038/icb.2012.9.
10. Kotenko SV, Gallagher G, Baurin VV, Lewis-Antes A, Shen M, Shah NK, Langer JA, Sheikh F, Dickensheets H, Donnelly RP. 2003. IFN-lambdas mediate antiviral protection through a distinct class II cytokine receptor complex. Nat Immunol 4:69–77. https://doi.org/10.1038/ni875.
11. Buck CB, Pastrana DV, Lowy DR, Schiller JT. 2004. Efficient intracellular assembly of papillomaviral vectors. J Virol 78:751–757. https://doi.org/10.1128/JVI.78.2.751-757.2004.
12. Sapp M, Day PM. 2009. Structure, attachment and entry of polyoma- and papillomaviruses. Virology 384:400–409. https://doi.org/10.1016/j.virol.2008.12.022.
13. Day PM, Schelhaas M. 2014. Concepts of papillomavirus entry into host cells. Curr Opin Virol 4:24–31. https://doi.org/10.1016/j.coviro.2013.11.002.
14. Joyce JG, Tung JS, Przysiecki CT, Cook JC, Lehman ED, Sands JA, Jansen KU, Keller PM. 1999. The L1 major capsid protein of human papillomavirus type 11 recombinant virus-like particles interacts with heparin and cell-surface glycosaminoglycans on human keratinocytes. J Biol Chem 274:5810–5822. https://doi.org/10.1074/jbc.274.9.5810.
15. Giroglou T, Florin L, Schafer F, Streeck RE, Sapp M. 2001. Human papillomavirus infection requires cell surface heparan sulfate. J Virol 75:1565–1570. https://doi.org/10.1128/JVI.75.3.1565-1570.2001.
16. Johnson KM, Kines RC, Roberts JN, Lowy DR, Schiller JT, Day PM. 2009. Role of heparan sulfate in attachment to and infection of the murine female genital tract by human papillomavirus. J Virol 83:2067–2074. https://doi.org/10.1128/JVI.02190-08.
17. Richards RM, Lowy DR, Schiller JT, Day PM. 2006. Cleavage of the papillomavirus minor capsid protein, L2, at a furin consensus site is necessary for infection. Proc Natl Acad Sci U S A 103:1522–1527. https://doi.org/10.1073/pnas.0508815103.

18. Kines RC, Thompson CD, Lowy DR, Schiller JT, Day PM. 2009. The initial steps leading to papillomavirus infection occur on the basement membrane prior to cell surface binding. Proc Natl Acad Sci U S A 106:20458–20463. https://doi.org/10.1073/pnas.0908502106.
19. Schelhaas M, Shah B, Holzer M, Blattmann P, Kuhling L, Day PM, Schiller JT, Helenius A. 2012. Entry of human papillomavirus type 16 by actin-dependent, clathrin- and lipid raft-independent endocytosis. PLoS Pathog 8:e1002657. https://doi.org/10.1371/journal.ppat.1002657.
20. Selinka HC, Giroglou T, Sapp M. 2002. Analysis of the infectious entry pathway of human papillomavirus type 33 pseudovirions. Virology 299:279–287. https://doi.org/10.1006/viro.2001.1493.
21. Day PM, Lowy DR, Schiller JT. 2003. Papillomaviruses infect cells via a clathrin-dependent pathway. Virology 307:1–11. https://doi.org/10.1016/S0042-6822(02)00143-5.
22. Day PM, Thompson CD, Schowalter RM, Lowy DR, Schiller JT. 2013. Identification of a role for the trans-Golgi network in human papillomavirus 16 pseudovirus infection. J Virol 87:3862–3870. https://doi.org/10.1128/JVI.03222-12.
23. Lipovsky A, Popa A, Pimienta G, Wyler M, Bhan A, Kuruvilla L, Guie MA, Poffenberger AC, Nelson CD, Atwood WJ, DiMaio D. 2013. Genome-wide siRNA screen identifies the retromer as a cellular entry factor for human papillomavirus. Proc Natl Acad Sci U S A 110:7452–7457. https://doi.org/10.1073/pnas.1302164110.
24. Popa A, Zhang W, Harrison MS, Goodner K, Kazakov T, Goodwin EC, Lipovsky A, Burd CG, DiMaio D. 2015. Direct binding of retromer to human papillomavirus type 16 minor capsid protein L2 mediates endosome exit during viral infection. PLoS Pathog 11:e1004699. https://doi.org/10.1371/journal.ppat.1004699.
25. Day PM, Baker CC, Lowy DR, Schiller JT. 2004. Establishment of papillomavirus infection is enhanced by promyelocytic leukemia protein (PML) expression. Proc Natl Acad Sci U S A 101:14252–14257. https://doi.org/10.1073/pnas.0404229101.
26. Pyeon D, Pearce SM, Lank SM, Ahlquist P, Lambert PF. 2009. Establishment of human papillomavirus infection requires cell cycle progression. PLoS Pathog 5:e1000318. https://doi.org/10.1371/journal.ppat.1000318.
27. Milligan GN, Bernstein DI. 1997. Interferon-gamma enhances resolution of herpes simplex virus type 2 infection of the murine genital tract. Virology 229:259–268. https://doi.org/10.1006/viro.1997.8441.
28. Parr MB, Parr EL. 1999. The role of gamma interferon in immune resistance to vaginal infection by herpes simplex virus type 2 in mice. Virology 258:282–294. https://doi.org/10.1006/viro.1999.9739.
29. Ashkar AA, Rosenthal KL. 2003. Interleukin-15 and natural killer and NKT cells play a critical role in innate protection against genital herpes simplex virus type 2 infection. J Virol 77:10168–10171. https://doi.org/10.1128/JVI.77.18.10168-10171.2003.
30. Schroder K, Hertzog PJ, Ravasi T, Hume DA. 2004. Interferon-gamma: an overview of signals, mechanisms and functions. J Leukoc Biol 75:163–189.
31. Ramana CV, Gil MP, Schreiber RD, Stark GR. 2002. Stat1-dependent and -independent pathways in IFN-gamma-dependent signaling. Trends Immunol 23:96–101. https://doi.org/10.1016/S1471-4906(01)02118-4.
32. Monath TP, Arroyo J, Levenbook I, Zhang ZX, Catalan J, Draper K, Guirakhoo F. 2002. Single mutation in the flavivirus envelope protein hinge region increases neurovirulence for mice and monkeys but decreases viscerotropism for monkeys: relevance to development and safety testing of live, attenuated vaccines. J Virol 76:1932–1943. https://doi.org/10.1128/JVI.76.4.1932-1943.2002.
33. Halfter UM, Derbyshire ZE, Vaillancourt RR. 2005. Interferon-gamma-dependent tyrosine phosphorylation of MEKK4 via Pyk2 is regulated by annexin II and SHP2 in keratinocytes. Biochem J 388:17–28. https://doi.org/10.1042/BJ20041236.
34. Cerqueira C, Samperio Ventayol P, Vogeley C, Schelhaas M. 2015. Kallikrein-8 proteolytically processes human papillomaviruses in the extracellular space to facilitate entry into host cells. J Virol 89:7038–7052. https://doi.org/10.1128/JVI.00234-15.
35. Bienkowska-Haba M, Williams C, Kim SM, Garcea RL, Sapp M. 2012. Cyclophilins facilitate dissociation of the human papillomavirus type 16 capsid protein L1 from the L2/DNA complex following virus entry. J Virol 86:9875–9887. https://doi.org/10.1128/JVI.00980-12.
36. Barry AO, Mege JL, Ghigo E. 2011. Hijacked phagosomes and leukocyte activation: an intimate relationship. J Leukoc Biol 89:373–382. https://doi.org/10.1189/jlb.0510270.
37. Montaner LJ, da Silva RP, Sun J, Sutterwala S, Hollinshead M, Vaux D, Gordon S. 1999. Type 1 and type 2 cytokine regulation of macrophage endocytosis: differential activation by IL-4/IL-13 as opposed to IFN-gamma or IL-10. J Immunol 162:4606–4613.
38. Pei G, Repnik U, Griffiths G, Gutierrez MG. 2014. Identification of an immune-regulated phagosomal Rab cascade in macrophages. J Cell Sci 127:2071–2082. https://doi.org/10.1242/jcs.144923.
39. Pei G, Schnettger L, Bronietzki M, Repnik U, Griffiths G, Gutierrez MG. 2015. Interferon-gamma-inducible Rab20 regulates endosomal morphology and EGFR degradation in macrophages. Mol Biol Cell 26:3061–3070. https://doi.org/10.1091/mbc.E14-11-1547.
40. Arunachalam B, Phan UT, Geuze HJ, Cresswell P. 2000. Enzymatic reduction of disulfide bonds in lysosomes: characterization of a gamma-interferon-inducible lysosomal thiol reductase (GILT). Proc Natl Acad Sci U S A 97:745–750. https://doi.org/10.1073/pnas.97.2.745.
41. Phan UT, Arunachalam B, Cresswell P. 2000. Gamma-interferon-inducible lysosomal thiol reductase (GILT). Maturation, activity, and mechanism of action. J Biol Chem 275:25907–25914.
42. Luster AD, Weinshank RL, Feinman R, Ravetch JV. 1988. Molecular and biochemical characterization of a novel gamma-interferon-inducible protein. J Biol Chem 263:12036–12043.
43. Haque MA, Li P, Jackson SK, Zarour HM, Hawes JW, Phan UT, Maric M, Cresswell P, Blum JS. 2002. Absence of gamma-interferon-inducible lysosomal thiol reductase in melanomas disrupts T cell recognition of select immunodominant epitopes. J Exp Med 195:1267–1277. https://doi.org/10.1084/jem.20011853.
44. Dautry-Varsat A, Ciechanover A, Lodish HF. 1983. pH and the recycling of transferrin during receptor-mediated endocytosis. Proc Natl Acad Sci U S A 80:2258–2262. https://doi.org/10.1073/pnas.80.8.2258.
45. Hopkins CR, Trowbridge IS. 1983. Internalization and processing of transferrin and the transferrin receptor in human carcinoma A431 cells. J Cell Biol 97:508–521. https://doi.org/10.1083/jcb.97.2.508.
46. Wiley HS, Herbst JJ, Walsh BJ, Lauffenburger DA, Rosenfeld MG, Gill GN. 1991. The role of tyrosine kinase activity in endocytosis, compartmentation, and down-regulation of the epidermal growth factor receptor. J Biol Chem 266:11083–11094.
47. Chang CP, Lazar CS, Walsh BJ, Komuro M, Collawn JF, Kuhn LA, Tainer JA, Trowbridge IS, Farquhar MG, Rosenfeld MG, Wiley SH, Gill GN. 1993. Ligand-induced internalization of the epidermal growth factor receptor is mediated by multiple endocytic codes analogous to the tyrosine motif found in constitutively internalized receptors. J Biol Chem 268:19312–19320.
48. French AR, Sudlow GP, Wiley HS, Lauffenburger DA. 1994. Postendocytic trafficking of epidermal growth factor-receptor complexes is mediated through saturable and specific endosomal interactions. J Biol Chem 269:15749–15755.
49. van Deurs B, Holm PK, Sandvig K. 1996. Inhibition of the vacuolar H(+)-ATPase with bafilomycin reduces delivery of internalized molecules from mature multivesicular endosomes to lysosomes in HEp-2 cells. Eur J Cell Biol 69:343–350.
50. Iversen TG, Skretting G, Llorente A, Nicoziani P, van Deurs B, Sandvig K. 2001. Endosome to Golgi transport of ricin is independent of clathrin and of the Rab9- and Rab11-GTPases. Mol Biol Cell 12:2099–2107. https://doi.org/10.1091/mbc.12.7.2099.
51. Stechmann B, Bai SK, Gobbo E, Lopez R, Merer G, Pinchard S, Panigai L, Tenza D, Raposo G, Beaumelle B, Sauvaire D, Gillet D, Johannes L, Barbier J. 2010. Inhibition of retrograde transport protects mice from lethal ricin challenge. Cell 141:231–242. https://doi.org/10.1016/j.cell.2010.01.043.
52. Kwak K, Jiang R, Wang JW, Jagu S, Kirnbauer R, Roden RB. 2014. Impact of inhibitors and L2 antibodies upon the infectivity of diverse alpha and beta human papillomavirus types. PLoS One 9:e97232. https://doi.org/10.1371/journal.pone.0097232.
53. Hindmarsh PL, Laimins LA. 2007. Mechanisms regulating expression of the HPV 31 L1 and L2 capsid proteins and pseudovirion entry. Virol J 4:19. https://doi.org/10.1186/1743-422X-4-19.
54. Day PM, Thompson CD, Lowy DR, Schiller JT. 2015. The HPV16 and MusPV1 papillomaviruses initially interact with distinct host components on the basement membrane. Virology 481:79–94. https://doi.org/10.1016/j.virol.2015.02.021.
55. Finnen RL, Erickson KD, Chen XS, Garcea RL. 2003. Interactions between papillomavirus L1 and L2 capsid proteins. J Virol 77:4818–4826. https://doi.org/10.1128/JVI.77.8.4818-4826.2003.
56. Der SD, Zhou A, Williams BR, Silverman RH. 1998. Identification of genes differentially regulated by interferon alpha, beta, or gamma using oligonucleotide arrays. Proc Natl Acad Sci U S A 95:15623–15628. https://doi.org/10.1073/pnas.95.26.15623.

57. Metz P, Dazert E, Ruggieri A, Mazur J, Kaderali L, Kaul A, Zeuge U, Windisch MP, Trippler M, Lohmann V, Binder M, Frese M, Bartenschlager R. 2012. Identification of type I and type II interferon-induced effectors controlling hepatitis C virus replication. Hepatology 56:2082–2093. https://doi.org/10.1002/hep.25908.
58. Sadler AJ, Williams BR. 2008. Interferon-inducible antiviral effectors. Nat Rev Immunol 8:559–568. https://doi.org/10.1038/nri2314.
59. Abend JR, Low JA, Imperiale MJ. 2007. Inhibitory effect of gamma interferon on BK virus gene expression and replication. J Virol 81: 272–279. https://doi.org/10.1128/JVI.01571-06.
60. De-Simone FI, Sariyer R, Otalora YL, Yarandi S, Craigie M, Gordon J, Sariyer IK. 2015. IFN-gamma inhibits JC virus replication in glial cells by suppressing t-antigen expression. PLoS One 10:e0129694. https://doi.org/10.1371/journal.pone.0129694.
61. Karupiah G, Xie QW, Buller RM, Nathan C, Duarte C, MacMicking JD. 1993. Inhibition of viral replication by interferon-gamma-induced nitric oxide synthase. Science 261:1445–1448. https://doi.org/10.1126/science.7690156.
62. Patterson JB, Thomis DC, Hans SL, Samuel CE. 1995. Mechanism of interferon action: double-stranded RNA-specific adenosine deaminase from human cells is inducible by alpha and gamma interferons. Virology 210:508–511. https://doi.org/10.1006/viro.1995.1370.
63. Lin HY, Yen PM, Davis FB, Davis PJ. 1997. Protein synthesis-dependent potentiation by thyroxine of antiviral activity of interferon-gamma. Am J Physiol 273:C1225–C1232.
64. Anderson SL, Carton JM, Lou J, Xing L, Rubin BY. 1999. Interferon-induced guanylate binding protein-1 (GBP-1) mediates an antiviral effect against vesicular stomatitis virus and encephalomyocarditis virus. Virology 256:8–14. https://doi.org/10.1006/viro.1999.9614.
65. Zamanian-Daryoush M, Mogensen TH, DiDonato JA, Williams BR. 2000. NF-kappaB activation by double-stranded-RNA-activated protein kinase (PKR) is mediated through NF-kappaB-inducing kinase and IkappaB kinase. Mol Cell Biol 20:1278–1290. https://doi.org/10.1128/MCB.20.4.1278-1290.2000.
66. Burdeinick-Kerr R, Griffin DE. 2005. Gamma interferon-dependent, non-cytolytic clearance of Sindbis virus infection from neurons in vitro. J Virol 79:5374–5385. https://doi.org/10.1128/JVI.79.9.5374-5385.2005.
67. Rhein BA, Powers LS, Rogers K, Anantpadma M, Singh BK, Sakurai Y, Bair T, Miller-Hunt C, Sinn P, Davey RA, Monick MM, Maury W. 2015. Interferon-gamma inhibits Ebola virus infection. PLoS Pathog 11: e1005263. https://doi.org/10.1371/journal.ppat.1005263.
68. Ronco LV, Karpova AY, Vidal M, Howley PM. 1998. Human papillomavirus 16 E6 oncoprotein binds to interferon regulatory factor-3 and inhibits its transcriptional activity. Genes Dev 12:2061–2072. https://doi.org/10.1101/gad.12.13.2061.
69. Li S, Labrecque S, Gauzzi MC, Cuddihy AR, Wong AH, Pellegrini S, Matlashewski GJ, Koromilas AE. 1999. The human papilloma virus (HPV)-18 E6 oncoprotein physically associates with Tyk2 and impairs Jak-STAT activation by interferon-alpha. Oncogene 18:5727–5737. https://doi.org/10.1038/sj.onc.1202960.
70. Park JS, Kim EJ, Kwon HJ, Hwang ES, Namkoong SE, Um SJ. 2000. Inactivation of interferon regulatory factor-1 tumor suppressor protein by HPV E7 oncoprotein. Implication for the E7-mediated immune evasion mechanism in cervical carcinogenesis. J Biol Chem 275:6764–6769.
71. Barnard P, McMillan NA. 1999. The human papillomavirus E7 oncoprotein abrogates signaling mediated by interferon-alpha. Virology 259: 305–313. https://doi.org/10.1006/viro.1999.9771.
72. Chang YE, Pena L, Sen GC, Park JK, Laimins LA. 2002. Long-term effect of interferon on keratinocytes that maintain human papillomavirus type 31. J Virol 76:8864–8874. https://doi.org/10.1128/JVI.76.17.8864-8874.2002.
73. Herdman MT, Pett MR, Roberts I, Alazawi WO, Teschendorff AE, Zhang XY, Stanley MA, Coleman N. 2006. Interferon-beta treatment of cervical keratinocytes naturally infected with human papillomavirus 16 episomes promotes rapid reduction in episome numbers and emergence of latent integrants. Carcinogenesis 27:2341–2353. https://doi.org/10.1093/carcin/bgl172.
74. Maher SG, Sheikh F, Scarzello AJ, Romero-Weaver AL, Baker DP, Donnelly RP, Gamero AM. 2008. IFNalpha and IFNlambda differ in their antiproliferative effects and duration of JAK/STAT signaling activity. Cancer Biol Ther 7:1109–1115. https://doi.org/10.4161/cbt.7.7.6192.
75. Feeley EM, Sims JS, John SP, Chin CR, Pertel T, Chen LM, Gaiha GD, Ryan BJ, Donis RO, Elledge SJ, Brass AL. 2011. IFITM3 inhibits influenza A virus infection by preventing cytosolic entry. PLoS Pathog 7:e1002337. https://doi.org/10.1371/journal.ppat.1002337.
76. Via LE, Fratti RA, McFalone M, Pagan-Ramos E, Deretic D, Deretic V. 1998. Effects of cytokines on mycobacterial phagosome maturation. J Cell Sci 111(Part 7):897–905.
77. Trost M, English L, Lemieux S, Courcelles M, Desjardins M, Thibault P. 2009. The phagosomal proteome in interferon-gamma-activated macrophages. Immunity 30:143–154. https://doi.org/10.1016/j.immuni.2008.11.006.
78. Yates RM, Hermetter A, Taylor GA, Russell DG. 2007. Macrophage activation downregulates the degradative capacity of the phagosome. Traffic 8:241–250. https://doi.org/10.1111/j.1600-0854.2006.00528.x.
79. Boukamp P, Petrussevska RT, Breitkreutz D, Hornung J, Markham A, Fusenig NE. 1988. Normal keratinization in a spontaneously immortalized aneuploid human keratinocyte cell line. J Cell Biol 106:761–771. https://doi.org/10.1083/jcb.106.3.761.
80. Suh KS, Mutoh M, Nagashima K, Fernandez-Salas E, Edwards LE, Hayes DD, Crutchley JM, Marin KG, Dumont RA, Levy JM, Cheng C, Garfield S, Yuspa SH. 2004. The organellular chloride channel protein CLIC4/mtCLIC translocates to the nucleus in response to cellular stress and accelerates apoptosis. J Biol Chem 279:4632–4641.
81. Roden RB, Greenstone HL, Kirnbauer R, Booy FP, Jessie J, Lowy DR, Schiller JT. 1996. In vitro generation and type-specific neutralization of a human papillomavirus type 16 virion pseudotype. J Virol 70:5875–5883.
82. Day PM, Pang YY, Kines RC, Thompson CD, Lowy DR, Schiller JT. 2012. A human papillomavirus (HPV) in vitro neutralization assay that recapitulates the in vitro process of infection provides a sensitive measure of HPV L2 infection-inhibiting antibodies. Clin Vaccine Immunol 19: 1075–1082. https://doi.org/10.1128/CVI.00139-12.
83. Rubio I, Seitz H, Canali E, Sehr P, Bolchi A, Tommasino M, Ottonello S, Muller M. 2011. The N-terminal region of the human papillomavirus L2 protein contains overlapping binding sites for neutralizing, cross-neutralizing and non-neutralizing antibodies. Virology 409:348–359. https://doi.org/10.1016/j.virol.2010.10.017.
84. Chen JW, Murphy TL, Willingham MC, Pastan I, August JT. 1985. Identification of two lysosomal membrane glycoproteins. J Cell Biol 101:85–95. https://doi.org/10.1083/jcb.101.1.85.
85. Cardone G, Moyer AL, Cheng N, Thompson CD, Dvoretzky I, Lowy DR, Schiller JT, Steven AC, Buck CB, Trus BL. 2014. Maturation of the human papillomavirus 16 capsid. mBio 5:e01104-14.
86. Day PM, Thompson CD, Buck CB, Pang YY, Lowy DR, Schiller JT. 2007. Neutralization of human papillomavirus with monoclonal antibodies reveals different mechanisms of inhibition. J Virol 81:8784–8792. https://doi.org/10.1128/JVI.00552-07.